Calpain mobilizes Atg9/Bif-1 vesicles from Golgi stacks upon autophagy induction by thapsigargin

Marcassa, Elena[1,#]; Raimondi, Marzia[1]; Anwar, Tahira[2]; Eskelinen, Eeva-Liisa[2]; Myers, Michael P.[3]; Triolo, Gianluca[3]; Schneider, Claudio[1] and Demarchi, Francesca[1]*

[1]C.I.B. National Laboratory, AREA Science Park, Padriciano 99 34012 Trieste, Italy; [2]Department of Biosciences University of Helsinki, PO Box 56, Helsinki, Finland; [3]International Centre for Genetic Engineering and Biotechnology AREA Science Park—Padriciano, Trieste, Italy

[#]Present address: Physiological Laboratory, Institute of Translational Medicine, University of Liverpool, Crown Street L69 3BX Liverpool, UK

*Corresponding author

Corresponding author mailing address: francesca.demarchi@lncib.it

Key words: calpain, CAPNS1, Bif-1, endophilin B1, autophagy, thapsigargin

Summary statement

ER stress triggers calpain dependent Bif-1 activation and induction of autophagosomes maturation by promoting ATG9/Bif-1 vesicles trafficking and fusion with LC3 bodies.

Abstract

CAPNS1 is essential for stability and function of the ubiquitous calcium dependent proteases micro- and milli-calpain. Upon the inhibition of the endoplasmic reticulum Ca2+ ATPase by 100nM thapsigargin, both micro-calpain and autophagy are activated in human U2OS osteosarcoma cells in a CAPNS1 dependent manner. As reported for other autophagy triggers, thapsigargin treatment induces Golgi fragmentation and fusion of Atg9/Bif-1 containing vesicles with LC3 bodies in control cells. On the opposite, CAPNS1 depletion is coupled to an accumulation of LC3 bodies and Rab5 early endosomes. Moreover, Atg9 and Bif-1 stay in the GM130-positive Golgi stacks and Atg9 fails to interact with the endocytic route marker transferrin receptor and to the core autophagic protein Vps34 in CAPNS1 depleted cells. Ectopic expression of a Bif-1 point mutant resistant to calpain processing is coupled to endogenous p62 and LC3-II accumulation. Altogether these data indicate that calpain allows Atg9/Bif-1 vesicles dynamic flux from the Golgi toward the budding autophagosome.

Introduction

The ubiquitous μ- and m-calpain are calcium dependent neutral cysteine proteases. They are composed by an 80-kD catalytic subunit, CAPN1 and CAPN2 respectively, and a common 28-kD regulatory subunit, CAPNS1 (Goll et al., 2003). Targeted disruption of CAPNS1 results in embryonic lethality at day 10 post-conception, as a consequence of severe defects in vascular development (Arthur et al., 2000). Calpain proteolytically process a number of specific substrates, in a tightly regulated manner, and therefore they exert pleiotropic functions within the living cell. For example, they modulate the adhesive complex dynamics in adherent cells (Bhatt et al., 2002), exerting both positive and negative functions in cellular adhesion and movement. Similarly, calpain can positively regulate autophagy (Demarchi et al., 2006) (Yoon et al., 2008; Escalante et al., 2013) and switch it off (Yousefi et al., 2006) (Menzies et al., 2015). Interestingly, autophagy is also involved in the modulation of cellular movements (Tuloup-Minguez et al., 2013) (Galavotti et al., 2013).

Ubiquitous calpains are associated with the endoplasmic reticulum and Golgi apparatus, both proposed as sites for autophagosome nucleation (Lamb et al., 2013). A number of environmental stimuli determine endoplasmic reticulum stress, and consequently induce autophagy (Ogata et al., 2006) (Ding et al., 2007) and trigger calpain activation. In particular, the sarco/endoplasmic reticulum Ca^{2+} ATPase (SERCA) is inhibited by thapsigargin in the nanomolar range, with consequent release of calcium from the endoplasmic reticulum coupled to calpain activation (Martinez et al., 2010) and autophagy initiation (Ogata et al., 2006). On the opposite, micromolar concentrations of thapsigargin inhibit intracellular calcium raise (Geiszt et al., 1995). Accordingly, 3-micromolar levels of thapsigargin lead to accumulation of mature autophagosomes by blocking autophagosomes fusion with the endocytic system (Ganley et al., 2011). The transmembrane protein Atg9 resides in the trans-Golgi network and late endosomes, and upon autophagy induction, it redistributes to peripheral cytoplasm where it co-localizes with LC3, in an ULK1 dependent manner(Yang et al., 2006). Moreover, Bax-interacting factor 1 Bif-1/Endophilin B1 promotes fission of Atg9 positive Golgi membranes and their trafficking towards the site of autophagosomes formation (Takahashi et al., 2011). Bif-1 is characterized by an N-Bin-amphiphysin-rvs domain, N-BAR, necessary for the binding to and curvature of the double lipid layer, and a carboxyl-terminal Src-homology 3 domain, SH3, that allows the interaction with proline-rich proteins (Pierrat et al., 2001). In particular, Bif-1 binding to UVRAG (ultraviolet irradiation resistant-associated

gene) protein mediates Beclin1 recruitment to the phagophore and, as a consequence, activation of autophagy (Takahashi et al., 2007.).

We previously demonstrated the requirement of CAPNS1 for autophagosomes formation in response to rapamycin in MEFs and human osteosarcoma U2OS cells. In this study we found the involvement of CAPNS1 in autophagy modulation in response to thapsigargin and we identified Bif-1 cleavage by calpain as a possible mechanism for the regulation of the early stages of autophagy by calpain. CAPNS1 depletion is coupled to a clear alteration in the distribution of the Golgi stacks, and a deregulation in the Atg9-Bif-1 dynamics upon autophagy induction by thapsigargin.

Results

Thapsigargin triggers calpain activation and autophagy in human U2OS cells.

We previously showed that CAPNS1 depleted human osteosarcoma U2OS cells and CAPNS1-/- MEFs fail to induce autophagosomes formation in response to nutrient deprivation, and rapamycin, the classic autophagy-inducing stimuli. (Demarchi et al., 2006). In order to identify the molecular basis of this impairment, we compared several steps of autophagosome formation in CAPNS1 depleted and control U2OS cells. 100nM thapsigargin was utilized as autophagy trigger, since this drug targets the endoplasmic reticulum, where calpain resides and autophagosomes originate from. In addition, thapsigargin was reported to activate both calpain and autophagy in various systems when used in the nanomolar range.

In order to evaluate calpain activation, 100 nM thapsigargin was added to control and shCAPNS1 U2OS cells and lysates were collected: at the following time points: 0, 10, 20, and 30 minutes. As shown in the western blot of Fig. 1A, thapsigargin can rapidly induce a reduction in CAPN1 precursor, coupled to an increase in active CAPN1. As expected, CAPN1 protein levels are sharply reduced in CAPNS1 depleted cells (Arthur et al., 2000). The increase of intracellular calcium after thapsigargin addition was verified using indo1, AM, a ratiometric calcium probe, and FACS analysis. A representative experiment is shown in Fig.1B. Thapsigargin triggers an increase of cytoplasmic calcium in both control and shCAPNS1 U2OS cells. Notably, basal calcium level is higher in CAPNS1 depleted cells respect to control cells. A similar phenotype was recently reported for CAPN3 depleted muscle cells (Toral-Ojeda et al., 2016).

In order to monitor autophagosome formation kinetics, control and shCAPNS1 U2OS cells were incubated with 100 nM thapsigargin for 0, 30, 60, 120 minutes. Next, the cell lysates were

collected and utilized for immunoblotting analysis of autophagy markers (Fig. 1C). In control cells, 120 min after thapsigargin addition, LC3-I is converted in its lipidated form LC3-II, while in shCAPNS1 cells the kinetics of LC3 lipidation appears faster and both LC3 forms accumulate. As expected for autophagy competent cells, p62 degradation couples LC3 lipidation in control cells. On the contrary, in shCAPNS1 cells, p62 levels remain almost stable, thus suggesting the existence of a block in autophagic clearance (Fig.1D). The basal levels of p62 are lower in shCAPNS1 cells respect to control ones. This might be due to an adaptation of the cells to cope with the clearance defect. As control for thapsigargin treatment efficacy, we checked the phosphorylation of inositol-requiring kinase, pIRE1, one of the effectors of the UPR. Collectively the data above described indicate that CAPNS1 depletion perturbs autophagosome clearance in response to thapsigargin treatment.

CAPNS1 depletion is coupled to an accumulation of LC3-II-positive structures.

In order to further characterize the effect of calpain on LC3 bodies' dynamics, live cells imaging experiments were performed. In particular, we monitored RFP-GFP-LC3 bodies upon thapsigargin treatment, both in control U2OS cells and in CAPNS1 depleted U2OS cells. RFP-GFP-LC3 bodies appear as yellow dots. These structures appear as red dots after their fusion with the lysosomes, due to the acidification that bleaches the GFP fluorescence. U2OS cells were seeded on plates and grown for 24 hours; then a commercial reagent designed for RFP-GFP-LC3 expression was added to the cells. 24 hours later, RFP-GFP-LC3 bodies were analysed in a 120 minutes time-lapse experiment. 100 nM thapsigargin was added to the cells after the first 15 minutes of acquisition. In CAPNS1 depleted cells, we noticed a progressive increase in the level of yellow dots as compared to control cells. This increase is evident in Fig. 2A, which shows the first and last images of representative time-lapse experiments, included as Movies 1,2. In order to quantify the RFP-GFP-LC3 bodies accumulation, the cells were fixed after two hours of incubation with 100 nM thapsigargin. Fig. 2B shows representative fields and the average number of yellow dots counted in three independent experiments. CAPNS1 depletion is coupled to an increase in the amount of yellow dots, in accordance with the increase in LC3-II shown in Fig. 1C. After treatment with thapsigargin, the number of yellow dots per cell is similar in control and CAPNS1 depleted cells. However, the dots are larger in CAPNS1 depleted cells, as it appears evident in the representative pictures of Fig.2B and in the time-lapse Movies 1,2. This result is consistent with the increase in LC3-II measured by quantification of western blots data shown in Fig.1C.

Early endosomes dynamics is perturbed in CAPNS1 depleted cells.

A large body of published data indicate the involvement of early endosomes in the process of autophagosomess formation (Puri et al., 2013) (Ao et al., 2014). We previously reported that CAPNS1 depletion causes impairment in autophagosomes formation and ectopic LC3 accumulation in endosome-like vesicles (Demarchi et al., 2006). As reported above, we found that CAPNS1 depletion influences RFP-GFP-LC3 trafficking in thapsigargin treated cells. Therefore, we expected a similar behaviour for Rab5 positive endosomes. To verify this hypothesis we applied the same video microscopy technology to monitor early endosomes behaviour upon thapsigargin treatment in live cells. Control and CAPNS1 depleted U2OS cells were treated with two commercial baculoviruses expressing the early endosome marker GFP-Rab5 and the endoplasmic reticulum marker KDEL-calreticulin. 24 hours later, a 50 minutes time-lapse experiment was performed using a confocal microscope. After the first 15 minutes of images acquisition, 100 nM thapsigargin was added to trigger calpain activation and induce autophagy. In both cell lines labelled endosomes move from the periphery of the cell toward the endoplasmic reticulum (Movies 3,4). Notably, in shCAPNS1 cells, stained endosomes accumulate and gather in a perinuclear region, (Fig. 3A lower panels). The accumulation is not observed in control cells (Fig. 3A upper panels). In order to further verify Rab5 behaviour and to quantify this phenotype, the same experiment was repeated and the cells were analysed after fixation on a coverslip. Corrected total cell fluorescence (CTCF) was measured using Image J software. As indicated in the graph of Fig. 3B, one hour hours after thapsigargin addition, almost 40% of CAPNS1 depleted cells are characterized by a CTFC $\geq 3x10^6$, showing a four fold increase in ectopic Rab5 levels with respect to control cells, confirming the data observed by time-lapse video microscopy. Notably, Rab5 stained endosomes accumulate in control cells treated with the calpain inhibitory peptide, calpeptine, just like upon CAPNS1 depletion (Supplementary Fig. S1). Collectively, these results demonstrate that calpain deficiency affects early endosomes dynamics, upon thapsigargin treatment. The accumulation of both RFP-GFP-LC3 and GFP-Rab5 in CAPNS1 depleted cells as compared to control ones, argues for a role of CAPNS1 in the early stages of autophagy.

CAPNS1 depletion is coupled to Golgi stacks redistribution.

The Golgi network represents one of the membrane sources for the formation and elongation of the phagophore, together with the ER and mitochondria (Matsunaga et al., 2010) (Yla-Anttila et al., 2009); (Hailey et al., 2010); (Hamasaki et al., 2013). In order to monitor the effect of CAPNS1 depletion on Golgi architecture, the endogenous cis-Golgi protein GM130 was

analysed by immunostaining in control U2OS cells, CAPNS1 depleted cells, and their derivatives with reintroduced CAPNS1. Fluorescence analysis reveals that in CAPNS1 depleted U2OS cells the Golgi network is condensed at one side of the nucleus, as compared to control cells, where its distribution is more scattered. Both distributions are observed in CAPNS1 rescued cells (Fig. 4A). The graph in Fig. 4B indicates the average of the percentage of cells with a canonical Golgi stacks distribution. Accordingly, also in mouse embryonic fibroblasts, CAPNS1 depletion is coupled to a perturbation in GM130 localization. Indeed, GM130 positive stacks are more tightly clustered near the nucleus. (Supplementary Fig. S2A). The Golgi apparatus was also analysed by transmission electron microscopy. In control cells Golgi stacks surround the nucleus, while in CAPNS1 depleted cells, the Golgi network is mainly gathered at one side of it, confirming the immunofluorescence data. (Supplementary Fig. S2B). Altogether these results indicate that calpain activity is important to regulate Golgi apparatus distribution. A disruption of the regular localization of Golgi stacks within the cytoplasm might have consequences also on the autophagic process.

CAPNS1 depletion is coupled to impairment of Atg9 traffic.

We hypothesized that calpain could regulate the delivery of membranes toward the site of autophagosome formation. Atg9 is the only transmembrane autophagic protein. Atg9 is localized in the Golgi apparatus and late endosome vesicles. Upon autophagy induction, it re-distributes in the peripheral cytoplasm where it co-localizes with LC3 (Young et al., 2006). Since calpain depletion affects both LC3 bodies' dynamics and Golgi stacks distribution, we investigated Atg9 and LC3 dynamics in our cellular system. Control and shCAPNS1 depleted U2OS cells were transiently co-transfected with GFP-Atg9 and HcRed-LC3 expression plasmids. 24 hours later, the cells were analysed by in vivo imaging in a 90 minutes time-lapse experiment. After the first 15 minutes of images acquisition, 100 nM thapsigargin was added to induce autophagy (Movies 5,6). In control cells Atg9 clearly localizes in a perinuclear region (Fig. 5A). After autophagy induction, Atg9 vesicles freely move and eventually fuse to LC3 dots (Fig. 5C). On the contrary, in shCAPNS1 cells, Atg9 positive vesicles are more stationary, they may stay in close proximity to LC3 bodies, but do not fuse with them (Fig. 5C). The degree of co-localization between HcRed-LC3-positive vacuoles and GFP-Atg9-positive vacuoles was quantified measuring the Pearson's coefficient of ≥10 cells under each condition in three independent experiments (fig.5B). Notably, unstained vesicles appear near the nucleus (Fig. 5A, right panels). A very similar LC3 staining was previously observed in cyclopentenone prostaglandin derivative treated HCT-116 cells (Kar et al., 2009). To further assess the

involvement of calpain in Atg9 vesicles dynamics, we followed a biochemical approach and investigated Atg9 interaction with TfR and Vps34 in presence or absence of CAPNS1. U2OS cells, stably expressing Flag-Atg9, were used to transiently deplete CAPNS1. CAPNS1 depleted and control cells were treated or not with 100 nM htapsigargin. One hour later, the cells were lysed and used to immunoprecipitate Flag-Atg9. Confirming published data, Atg9 interacts with TfR in control cells. Notably, in CAPNS1 depleted cells this interaction is less evident, and it is further reduced upon autophagy induction with 100 nM thapsighargin (Fig. 5D). In control cells, Atg9 interacts with Vps34, a component of the class III PI3K complex, underling the importance of Atg9 in the initial steps of the autophagic process (Fig. 5C). Notably, VPS34 does not co-immunoprecipitate with Atg9 in CAPNS1 depleted cell lysates. Taken together, these data indicate that calpain allows trafficking of Atg9 toward the nascent autophagosome.

CAPNS1 depletion prevents trafficking of Atg9 and Bif-1 containing vesicles upon autophagy induction by thapsigargin.

Bif-1 interacts directly with the double lipid layer of membranes, trough its N-BAR domain, promoting Golgi tubules fission and the delivery of Atg9 vesicles to the nascent autophagosome upon autophagy induction (Takahashi et al., 2011). As a first approach to evaluate any effect of calpain on Bif-1, we checked its distribution respect to LC3, in presence or absence of CAPNS1. AmCyan-Bif1 and HcRed-LC3 expressing constructs were transiently transfected in control and CAPNS1 depleted U2OS cells. As it is shown in Figs. 6A,B, CAPNS1 depletion is coupled to an accumulation of Bif-1 positive aggregates near the nucleus, when compared to control cells.

In order to study the effect of CAPNS1 depletion on Atg9 and Bif-1 trafficking, we utilized a U2OS cell line stably expressing Flag-Atg9 and transiently transfected with AmCyan-Bif-1 expressing plasmid. CAPNS1 specific or control siRNA were transiently transfected in this system and the cells were treated or not for one hour with 100 nM thapsigargin to induce autophagy. Flag-Atg9, AmCyan-Bif-1, and endogenous GM130 were analysed by fluorescence microscopy. Upon thapsigargin treatment, Bif-1/Atg9 double positive vesicles move away from endogenous GM130 in control cells (Fig. 6C, upper panels). On the contrary, in CAPNS1 depleted cells, Bif-1 and Atg9 remain on GM-130 positive Golgi membranes (Fig. 6C, lower panels). The graph in Fig. 6D indicates the average number of cells where Flag-Atg9/AmCyan-Bif-1 double positive vesicles are stained also by anti-GM130 antibody. Collectively, these data indicate that calpain allows the fission of Bif-1/Atg9 vesicles from the Golgi apparatus.

Bif-1 protein is cleaved by calpain.

By means of bio-informatics tools based on the Multiple Kernel Learning algorithms, it is possible to identify putative calpain cleavage sites on an aminoacid sequence (DuVerle et al., 2011). The two sites with the highest calpain cleavage score on Bif-1 are located between the BAR domain and the SH3 domain at aminoacids 296 and 290. Notably, potential calpain cleavage sites are present also on Atg9 protein sequence. To verify the predicted cleavage sites on Bif-1, we performed an in-vitro calpain cleavage assay. Wild-type-Bif-1, Bif-1 lacking the SH3 domain, and the SH3 domain of Bif-1 (Fig. 7A) were produced as [35S]-methionine-labelled proteins by in vitro transcription and translation. NF-κB1 p50 was produced as a positive and negative control for the cleavage experiment. The radioactive products were incubated for 0, 2 and 10 minutes with commercial micro-calpain. As indicated by the arrows in Fig. 7B, a cleavage products originates both from Bif-1 wt and Bif-1 ΔSH3, but not from Bif-1 SH3. EGTA, an inhibitor of calpain, prevents Bif-1 digestion. These results demonstrate that micro-calpain cuts Bif-1 outside the SH3 domain. Moreover, since after calpain cleavage, the decrease in size of both full length and Bif-1-ΔSH3 is comparable, we predict that the cleavage occurs near the N-terminal end of the protein. In order to test this hypothesis, Bif-1 wt-myc and Bif-1-ΔSH3-myc at 0 and 10 minutes after calpain digestion and respective EGTA containing controls were separated on gel and analysed by immunoblot using anti-myc tag or anti-Bif-1 antibodies (Fig. 7C). The anti-myc antibody recognizes a digestion product of the same molecular weight of the fragment visualized by autoradiography (hollow arrow). On the other hand, the anti-Bif-1 antibody detects also two lower molecular weight bands (solid arrows). On the basis of their molecular weight, we speculate they could derive from subsequent processing that remove the SH3 domain or both the SH3 domain, and the variable region. This hypothesis is schematized in the cartoon of Fig. 7C. In vitro calpain cleavage assays using GST-Bif-1 as a substrate, further suggest that a first cleavage occurs at the very N-terminal end of Bif-1 (Supplementary Fig. S3). We failed to detect any cleavage product of endogenous Bif-1 analysing total cellular lysates by western blot. We hypothesize that the cleavage products have a very short life within the cell, as described for other calpain targets, thus allowing a tightly controlled and transient activity of the active protein.

Overexpression of E28A Bif-1 is coupled to autophagic block.

Using the freely available software described by the group of Sorimachi[29], we searched for cleavage sites in the first 37 aminoacids, corresponding to the first domain of Bif-1, which is required for membrane binding. By means of this bioinformatics tool, we found that glutamic

acid 29 is the best candidate for calpain cleavage. Therefore, we produced one E28A Bif-1 point mutant. We selected aminoacid 28 since it corresponds to position P2 respect to the putative cleavage site at lysine 29 identified by in silico analysis, and is therefore essential for site selection. As shown in Fig. 8A, the mutant is resistant to calpain proteolytic processing in the N-terminal region. Notably, the mutant protein is completely degraded by calpain in vitro. This result suggests that, upon loss of the preferential processing site, calpain can cleave Bif-1 at several sites, originating unstable peptides. In order to investigate whether overexpression of E28A Bif-1 might impact autophagy in the cell, even in the presence of endogenous Bif-1, we employed a cell line characterized by a high level of basal autophagic flux. In particular, we selected H1299, a non small cell lung carcinoma cell line. E28A Bif-1-myc and wild type Bif-1-myc constructs were transfected in H1299 cells and 24 hours later, incubated or not with thapsigargin for one hour. Next, cellular lysates were prepared and analysed by immunoblot. As shown in Fig. 8B, overexpression of each point mutant leads to a sharp accumulation of both p62, and LC3-II, suggestive of impaired autophagy. Thapsigargin treatment in this cell line does not further increase LC3 lipidation, possibly because the autophagic flux is already intense in this cell line. Indeed, as shown in the representative images of Fig. 8C, endogenous LC3 dots, stained in green, are already present in basal conditions, confirming the high autophagic activity of the H1299 cell line. Notably, endogenous LC3 dots are more numerous and appear to form larger structures in the cells overexpressing E28A Bif-1.

Altogether these results demonstrate that a point mutation of Bif-1 at glutamic acid 28 results in the impairment of calpain mediated processing of Bif-1 N-terminal domain. Furthermore, overexpression of E28A Bif-1 in H1299 cells is coupled to accumulation of p62 and LC3 aggregates.

Discussion

A large body of studies indicate that in mammalian cells the endoplasmic reticulum is a site for autophagosome nucleation [20] [Hamasaki, 2013 #10}. Moreover, the endocytic network contributes to phagophore formation and expansion as well as autophagosome maturation (Moreau et al., 2011) (Lamb et al., 2013). Notably, Atg9, the only known transmenbrane autophagic protein is present both in the endosomal compartment, and Golgi apparatus, both described as autophagosome membrane sources (Orsi et al., 2012) (Puri et al., 2013). The fission of Atg9 containing vesicles from the Golgi stacks involves the endophilin Bif-1, that also plays a critical role in vesicle formation for coat protein I (COPI)-mediated retrograde transportation from the trans-Golgi network to the endoplasmic reticulum (Yang et al., 2006). Here we describe the requirement of CAPNS1 for the trafficking of Atg9/Bif-1 bearing vesicles from the Golgi apparatus, and for the interaction of Atg9 with the autophagic essential kinase Vps34. The fusion of Bif-1/Atg9 containing vesicles with LC3 bodies budding from the ER, may allow membrane bending and formation of the mature double membrane autophagosome (Takahashi et al., 2007) (Takahashi et al., 2011). It is well established that calpain mediated processing can confer novel functions to their substrates (Sorimachi et al., 2011). Our study identified a calpain cleavage site on the N-terminal region of Bif-1. We hypothesize that calpain-mediated processing of Bif-1 N-terminus may remove the anchorage that retains outgoing vesicles in the Golgi apparatus. Therefore, this cut may be instrumental for the fission of tubular elements containing Atg9 from the Golgi apparatus, and subsequent fusion with LC3 vesicles coming from the endoplasmic reticulum. Interestingly, in macrophages, a LC3 associated phagocytosis was described as a mechanism involving many autophagic players, but without the formation of a double membrane (Martinez et al., 2015). Possibly, a similar pathway may exist also in other cell types allowing an alternative way for membrane trafficking involving LC3. We also found other potential calpain cleavage sites by in vitro studies. We speculate that subsequent cleavages that remove the SH3 domain may allow the removal of Bif-1 and its binding partners from the mature autophagosome. An alternative mechanism for Bif-1 regulation by calpain was proposed by Wong et al. (Ganley et al., 2011). They studied Bif-1-dependent autophagy induction in neurons. According to their study, calpain might cleave p35 to relase p25, which activates Cdk5 and this in turn phosphorylates Bif-1 at T145, being a prerequisite for proper Bif-1 activity. Possibly, both calpain dependent CDK5 mediated phosphorylation and calpain mediated processing may occur sequentially, as it was reported for talin modulation.

Time-lapse analysis of CAPNS1 depleted U2OS cells reveals an LC3 staining coupled to cytoplasmic vacuolation upon thapsigargin treatment. A very similar pattern was previously observed by others in HCT-116 upon cyclpentone prostaglandin derivative treatment (Kar et al., 2009). The vacuolation was reported to be a consequence of ER stress-induced ER dilation, subsequently leading to cell death. Also in our study, vacuolation is coupled to ER stress induced by thapsigargin. Moreover, we previously reported increased cell death in CAPNS1 depleted cells upon damage/stress (Demarchi et al., 2006).

We observed an enlargement of the endosome compartment upon thapsigargin treatment in CAPNS1 depleted cells. Interestingly, enlarged vesicles containing the Rab5 effector EEA1 were described in Bif-1 depleted cells (Wan et al., 2008). This similar phenotype may suggest that calpain is important also for Bif-1 role in endosome trafficking and function. Notably, a protein complex consisting of TIP30, Bif-1, and ACSL4 is crucial for moving Rab5 and v-ATPase to endosome precursors (Zhang et al., 2011).

Other studies indicate a negative role for calpain in the autophagic process (Menzies et al., 2015), but this is not surprising, given the pleiotropic functions of these processing proteases, and the tightly regulated transient activation of these enzymes. Indeed, calpain was reported to have both positive and negative roles in cellular movement. As far as autophagy is concerned, calpain may exert the cleavage of Bif-1 to allow scission of Golgi components and their targeting to the nascent autophagosomes. Subsequently, or in presence of excessive stress, it may cleave essential proteins such as Atg5 (Yousefi et al., 2006) and switch off the process. We propose that upon transient activation of calpain in response to cellular stressors, Bif-1/Atg9 bearing vesicles move from the Golgi network toward the site of autophagosome formation, where they interact with Class III PI3K Vps34. Subsequently, Atg9 is recycled through the endocytic pathway, and it interacts with the transferrin receptor. When the cellular stress becomes overwhelming, calpain hyperactivation leads to inhibition of autophagic players and to calpain inhibition by calpastatin. At this point, an alternative pathway involving LC3 bodies becomes prevalent over macroautophagy.

Materials and Methods

Plasmid and Reagents. The pAmCyan-N1-Bif1, pGEX-4T1-Bif-1, pEF6-Bif-1wt-Myc-HisA, pEF6-Bif-1dSH3-Myc and the pEF6-Myc-HisA-Bif-1S were a kind gift of Dr. Hong-Gang Wang. pHAGE-N-GFP-ATG9 and MSCV-Tet-FLAG-HA-IRES-PURO-ATG9 were generously provided by Dr. Ivan Dikic. Thapsigargin and Isopropil-β-D-1-tiogalattopiranoside (IPTG) were bought from Sigma. Indo1, AM was purchased from ThermoFisher Scientific. Antibodies were obtained from the following sources: rabbit anti-ATG9 (Cat.NBP195342, Clone 9B11); mouse anti-Bif-1 (Cat. NBP2-24733, Clone 30A882.1.1); and rabbit anti-pIRE (Cat. NB1002323); from Novus Biologicals; mouse anti-Flag (Cat. F3165, Clone M2), rabbit anti-Actin (Cat. A2066), and mouse anti-CAPNS1(Cat. C0230, Clone 28F3) from Sigma; mouse anti-GM130 (Cat. 610822, Clone 35) and mouse anti-p62 (Cat. 610832, Clone 3) from BD Transduction Laboratories; mouse anti-Myc-Tag (Cat. 2276, Clone 9B11) from Cell Signaling; goat anti-CAPN1 precursor (sc-7531, Clone N-19) and goat anti-CD71(TfR) (sc-32272, Clone 3B82A1) from Santa Cruz; rabbit anti-active CAPN1 (ab28257) from Abcam; rabbit anti-Vps34 (Cat. 382100) from ThermoFisher Scientific. LC3 antibodies were purified from rabbit serum after immunization with GST-LC3 according to standard procedures. siRNA targeting CAPNS1 was purchased from Eurofins MWG Operon (Germany): the pool of four siRNAs targeting CAPNS1 (1-GAG CAU CUC UAU AAC AUG AUU TT, 2-CCA CAG AAC UCA UGA ACA UUU TT, 3-UCA GGG ACC AUU UGC AGU AUU TT, 4-GAA GAU GGA UUU UGA CAA CUU TT). The Baculovirus reagents, RFP-GFP-LC3, GFP-Rab5a and GFP-E1-alpha-pyrivate-dehydrogenase, were purchased from ThermoFisher Scientific. For the in-vitro transcription and translation of radio-marked proteins TnT T7 Quick Coupled Transcription/Translation System (Promega) was used.

Cell Culture, transfection and sh-RNA mediated gene silencing. All the cells are routinely checked for contamination. U2OS cells were obtained from ATCC and recently authenticated. They were grown in Dulbecco's modified Eagle's medium (DMEM) low glucose, supplemented with 10% FCS, 1% penicillin/streptomycin (Lonza) and L-glutamine. U2OS pRS-control and pRS-shCAPNS1 (Raimondi et al., 2016) were produced according to standard procedures. For cell infections: 293GP packaging cells were transfected with the calcium-phosphate method with pRetroSuper-shCAPNS1 or vector alone, after 72 hours the supernatant was harvested, filtered and added to U2OS cells. The infected cells were selected by the addition of puromycin and after 7 days the expression of CAPNS1 was checked by western blot. The same protocol was used to produce U2OS cells stably expressing HA-Flag-ATG9. For the production of the shCAPNS1 stable cell line with the reintroduction of calpain small subunit, the U2OS cells

describe above were infected with a pwzL vector expressing CAPNS1. 293T cells were grown in DMEM high glucose, supplemented with 10% FCS and 1% penicillin/streptomycin. Wild-type, CAPNS1-/- and *rescued* mouse embryonic fibroblasts (Arthur et al., 2000) were a kind gift of Dr. Peter A. Greer (Ontario, Canada); cells were grown in DMEM high glucose, supplemented with 10% fetal calf serum (FCS), 1% penicillin/streptomycin and Non-Essential Aminoacids solutions 100X (Sigma). For transient transfection and silencing, TransIT-LT1 transfection reagent (Mirus) and Lipofectamine RNAiMAX (Invitrogen) were used respectively, according to the manufacturer's instructions.

Kinetic analysis of intracellular calcium concentration. U2OS cells were incubated for 30 minutes at 37°C with 2.5uM Indo1-AM in DMEM-1%FCS. Next, the cells were washed and incubated in DMEM-1%FCS for 20 min at room temperature. The samples were then run through the flow cytometer BD LSRFortessa Analyzer for three minutes and then for additional four minutes after thapsigargin (100nM) addition. FlowJo software version 8.8.7 was used to analyze the data. Indo-1 emission peak shifts from 485 nm (indo-blue) for unbound dye to 405 nm (indo-violet) when the indo-1 molecule is bound to calcium. Mean intracellular calcium concentration is quantified in terms of the ratio of 405 nm/485 nm indo-1emission peaks. Moving average was applied to increase the signal to noise ratio, as previously described (MacFarlane et al., 2010).

Western Blot analysis and Immunoprecipitation. Cell lysates were obtained in 50 mM Tris-HCl pH 7.5; 150 mM NaCl, 5 mM EDTA, 1% Triton X-100, supplemented with 0.5 mM NaF, 2 mM EGTA, 1 mM Sodium orthovanadate and complete protease inhibitor cocktail (Sigma). Lysates were clarified by centrifugation for 10 min at 4°C and protein concentrations were assessed using Bradford protein assay (BioRad Laboratories). Samples containing equal amounts of proteins were boiled in SDS sample buffer, resolved using SDS-PAGE and transferred to nitrocellulose membranes. The blots were then probed with the appropriate antibodies. Before immunoprecipitation, U2OS cells stably expressing HA-Flag-ATG9 were transiently silenced for CAPNS1 for 3 days, and then treated for 1 h with 100 nM thapsigargin. Whole cell lysates in 20 mM CHAPS, 125 mM NaCl, 50 mM TrisHCl, pH 7.5, supplemented with 0.5 mM NaF, 1 mM Sodium orthovanadate, complete protease inhibitor cocktail (Sigma), were incubated for 2 h with anti-Flag antibody or with the anti-Myc antibody as negative control. Subsequently, protein G (GE Healthcare Life Sciences) was added for 2 h at 4°C. Samples were subjected to SDS-PAGE and immunoblotting.

Confocal Microscopy and live-cell imaging. U2OS cells transiently transfected with GFP and AmCyan tagged expression constructs or treated with commercial Baculovirus reagents were fixed on coverslips with 3% PFA for 20 min., washed with 0,1 M glycine in PBS and stained with Hoechst solution or propidium iodide for 5 min at room temperature. For immunofluorescence, after fixation with PFA, the cells were permeabilized with 0,1% Triton-X100 in PBS for 5 min., and blocked in PBS containing 5% BSA for 30 min. at room temperature; then the slides were incubated with the appropriate antibodies (1:100) for 2 h at 37°C. Following 3 washings with PBS, samples were stained with secondary antibodies for 1 h at room temperature. Images were acquired with LSM510 confocal microscope (Zeiss), and processed using ImageJ software, freely available on the net. Imaging of live U2OS cells, grown on Nunc Glass Base dishes (Thermo Scientific) was performed on LSM510 confocal microscope (Zeiss), equipped with a cells incubator. Images were acquired every 2 min.

Electron Microscopy: Cells monolayers were fixed in 2% glutaraldehyde in 0,2 M Hepes buffer, pH 7.4, for 1 h at room temperature. Next the cells were incubated in 1% osmium tetroxide in 0,1 M sodium cacodylate buffer, pH 7.4, with the addition of 15 mg/mL of potassium ferrocyanide, for 1 hour at room temperature. Then slides were dehydrated in a graded series of ethanol and embedded in Epon using routine procedures. Approximately 60-nm sections were cut and stained using uranyl acetate and lead citrate and were examined with a transmission electron microscope (Jeol JEM-1400).

Expression and purification of GST-Bif-1. GST-Bif-1 was expressed by pGEX-4T-1 plasmid in BL21de3 strain of *Escherichia coli*. Briefly, transformed cells were grown in Luria Bertani medium containing 100 μg/mL ampicillin at 37°C to an $A_{600\ nm}$ 0,8; then 1 mM IPTG was added to induce protein expression at 37°C for 3 h. Cells were lysed in PBS, pH 7.4, supplemented with 0.5 mM NaF, 2 mM EGTA, 1 mM Sodium orthovanadate and complete protease inhibitor cocktail, by sonication and centrifuged at 8000 xg for 30 min. The resulting supernatant was incubated with Glutathione Sepharose 4B (GE Healthcare) at 4°C for 1 h and then washed three times with PBS. The protein was eluted with 10 mM reduced glutathione in 50 mM Tris-HCl, pH 8.

In vitro cleavage assay. ^{35}S-labelled in-vitro transcribed/translated proteins were produced by standard procedures and incubated with micro-calpain on ice in 10 mM Tris, pH 7.5, 1.5 mM DTT, 750 μM $CaCl_2$ as described (Cataldo et al., 2013). Reactions were terminated at the indicated time points by adding SDS-PAGE loading buffer and analysed on SDS-PAGE.

Statistical Analysis. Results are expressed as means ± standard deviations of at least three independent experiments. Statistical analysis was performed using two-tailed Student's t test or two-way ANOVA with the minimal level of significance set at $p<0,05$.

Acknowledgements

We thank the Electron Microscopy Unit at the Institute of Biotechnology, University of Helsinki, for access to their facilities, and Arja Strandel for technical help. We are grateful to Dr. Y. Takahashi and Prof. H-G.Wang from Penn State College of Medicine for providing Bif-1 constructs, and to Prof. I. Dikic from IBCII Frankfurt for sharing Atg9 constructs.

Competing interests

No competing interests declared.

Authors contribution

Conceptualization: D.F.; Supervision: D.F., E.E.; Investigation and Formal analysis: M.E., M.M., A.T., T.G., M.M.; Funding acquisition: D.F., S.C., E.E.; Writing: D.F.

Funding

This work was supported by a Project funded under the Cross-Border Cooperation Programme Italy-Slovenia 2007-2013 by the European Regional Development Fund and national funds to F. Demarchi; funds from the Academy of Finland (ELE), and Magnus Ehrnrooth Foundation, Finland (TA) to E.L.Eskelinen and a FIRB grant CINECA RBAPMLP2W, and CTN01_00177_817708 to C. Schneider.

References

Ao, X., Zou, L. and Wu, Y. (2014). Regulation of autophagy by the Rab GTPase network. *Cell Death Differ* **21**, 348-358.

Arthur, J. S., Elce, J. S., Hegadorn, C., Williams, K. and Greer, P. A. (2000). Disruption of the murine calpain small subunit gene, Capn4: calpain is essential for embryonic development but not for cell growth and division. *Mol Cell Biol* **20**, 4474-4481.

Bhatt, A., Kaverina, I., Otey, C. and Huttenlocher, A. (2002). Regulation of focal complex composition and disassembly by the calcium-dependent protease calpain. *J Cell Sci* **115**, 3415-3425.

Cataldo, F., Peche, L. Y., Klaric, E., Brancolini, C., Myers, M. P., Demarchi, F. and Schneider, C. (2013). CAPNS1 regulates USP1 stability and maintenance of genome integrity. *Mol Cell Biol* **33**, 2485-2496.

Demarchi, F., Bertoli, C., Greer, P. A. and Schneider, C. (2005). Ceramide triggers an NF-kappaB-dependent survival pathway through calpain. *Cell Death Differ* **12**, 512-522.

Demarchi, F., Bertoli, C., Copetti, T., Tanida, I., Brancolini, C., Eskelinen, E. L. and Schneider, C. (2006). Calpain is required for macroautophagy in mammalian cells. *J Cell Biol* **175**, 595-605.

Ding, W. X., Ni, H. M., Gao, W., Hou, Y. F., Melan, M. A., Chen, X., Stolz, D. B., Shao, Z. M. and Yin, X. M. (2007). Differential effects of endoplasmic reticulum stress-induced autophagy on cell survival. *J Biol Chem* **282**, 4702-4710.

DuVerle, D. A., Ono, Y., Sorimachi, H. and Mamitsuka, H. (2011). Calpain cleavage prediction using multiple kernel learning. *PLoS One* **6**, e19035.

Escalante, A. M., McGrath, R. T., Karolak, M. R., Dorr, R. T., Lynch, R. M. and Landowski, T. H. (2013). Preventing the autophagic survival response by inhibition of calpain enhances the cytotoxic activity of bortezomib in vitro and in vivo. *Cancer Chemother Pharmacol* **71**, 1567-1576.

Galavotti, S., Bartesaghi, S., Faccenda, D., Shaked-Rabi, M., Sanzone, S., McEvoy, A., Dinsdale, D., Condorelli, F., Brandner, S., Campanella, M. et al. (2013). The autophagy-associated factors DRAM1 and p62 regulate cell migration and invasion in glioblastoma stem cells. *Oncogene* **32**, 699-712.

Ganley, I. G., Wong, P. M., Gammoh, N. and Jiang, X. (2011). Distinct autophagosomal-lysosomal fusion mechanism revealed by thapsigargin-induced autophagy arrest. *Mol Cell* **42**, 731-743.

Geiszt, M., Kaldi, K., Szeberenyi, J. B. and Ligeti, E. (1995). Thapsigargin inhibits Ca2+ entry into human neutrophil granulocytes. *Biochem J* **305 (Pt 2)**, 525-528.

Goll, D. E., Thompson, V. F., Li, H., Wei, W. and Cong, J. (2003). The calpain system. *Physiol Rev* **83**, 731-801.

Hailey, D. W., Rambold, A. S., Satpute-Krishnan, P., Mitra, K., Sougrat, R., Kim, P. K. and Lippincott-Schwartz, J. (2010). Mitochondria supply membranes for autophagosome biogenesis during starvation. *Cell* **141**, 656-667.

Hamasaki, M., Furuta, N., Matsuda, A., Nezu, A., Yamamoto, A., Fujita, N., Oomori, H., Noda, T., Haraguchi, T., Hiraoka, Y. et al. (2013). Autophagosomes form at ER-mitochondria contact sites. *Nature* **495**, 389-393.

Kar, R., Singha, P. K., Venkatachalam, M. A. and Saikumar, P. (2009). A novel role for MAP1 LC3 in nonautophagic cytoplasmic vacuolation death of cancer cells. *Oncogene* **28**, 2556-2568.

Lamb, C. A., Dooley, H. C. and Tooze, S. A. (2013). Endocytosis and autophagy: Shared machinery for degradation. *Bioessays* **35**, 34-45.

MacFarlane, A. W. t., Oesterling, J. F. and Campbell, K. S. (2010). Measuring intracellular calcium signaling in murine NK cells by flow cytometry. *Methods Mol Biol* **612**, 149-157.

Martinez, J., Malireddi, R. K., Lu, Q., Cunha, L. D., Pelletier, S., Gingras, S., Orchard, R., Guan, J. L., Tan, H., Peng, J. et al. (2015). Molecular characterization of LC3-associated phagocytosis reveals distinct roles for Rubicon, NOX2 and autophagy proteins. *Nat Cell Biol* **17**, 893-906.

Martinez, J. A., Zhang, Z., Svetlov, S. I., Hayes, R. L., Wang, K. K. and Larner, S. F. (2010). Calpain and caspase processing of caspase-12 contribute to the ER stress-induced cell death pathway in differentiated PC12 cells. *Apoptosis* **15**, 1480-1493.

Matsunaga, K., Morita, E., Saitoh, T., Akira, S., Ktistakis, N. T., Izumi, T., Noda, T. and Yoshimori, T. (2010). Autophagy requires endoplasmic reticulum targeting of the PI3-kinase complex via Atg14L. *J Cell Biol* **190**, 511-521.

Menzies, F. M., Garcia-Arencibia, M., Imarisio, S., O'Sullivan, N. C., Ricketts, T., Kent, B. A., Rao, M. V., Lam, W., Green-Thompson, Z. W., Nixon, R. A. et al. (2015). Calpain inhibition mediates autophagy-dependent protection against polyglutamine toxicity. *Cell Death Differ* **22**, 433-444.
Moreau, K., Ravikumar, B., Renna, M., Puri, C. and Rubinsztein, D. C. (2011). Autophagosome precursor maturation requires homotypic fusion. *Cell* **146**, 303-317.
Ogata, M., Hino, S., Saito, A., Morikawa, K., Kondo, S., Kanemoto, S., Murakami, T., Taniguchi, M., Tanii, I., Yoshinaga, K. et al. (2006). Autophagy is activated for cell survival after endoplasmic reticulum stress. *Mol Cell Biol* **26**, 9220-9231.
Orsi, A., Razi, M., Dooley, H. C., Robinson, D., Weston, A. E., Collinson, L. M. and Tooze, S. A. (2012). Dynamic and transient interactions of Atg9 with autophagosomes, but not membrane integration, are required for autophagy. *Mol Biol Cell* **23**, 1860-1873.
Pierrat, B., Simonen, M., Cueto, M., Mestan, J., Ferrigno, P. and Heim, J. (2001). SH3GLB, a new endophilin-related protein family featuring an SH3 domain. *Genomics* **71**, 222-234.
Puri, C., Renna, M., Bento, C. F., Moreau, K. and Rubinsztein, D. C. (2013). Diverse autophagosome membrane sources coalesce in recycling endosomes. *Cell* **154**, 1285-1299.
Raimondi, M., Marcassa, E., Cataldo, F., Arnandis, T., Mendoza-Maldonado, R., Bestagno, M., Schneider, C. and Demarchi, F. (2016). Calpain restrains the stem cells compartment in breast cancer. *Cell Cycle* **15**, 106-116.
Sorimachi, H., Hata, S. and Ono, Y. (2011). Impact of genetic insights into calpain biology. *J Biochem* **150**, 23-37.
Takahashi, Y., Meyerkord, C. L., Hori, T., Runkle, K., Fox, T. E., Kester, M., Loughran, T. P. and Wang, H. G. (2011). Bif-1 regulates Atg9 trafficking by mediating the fission of Golgi membranes during autophagy. *Autophagy* **7**, 61-73.
Takahashi, Y., Coppola, D., Matsushita, N., Cualing, H. D., Sun, M., Sato, Y., Liang, C., Jung, J. U., Cheng, J. Q., Mule, J. J. et al. (2007). Bif-1 interacts with Beclin 1 through UVRAG and regulates autophagy and tumorigenesis. *Nat Cell Biol* **9**, 1142-1151.
Toral-Ojeda, I., Aldanondo, G., Lasa-Elgarresta, J., Lasa-Fernandez, H., Fernandez-Torron, R., Lopez de Munain, A. and Vallejo-Illarramendi, A. (2016). Calpain 3 deficiency affects SERCA expression and function in the skeletal muscle. *Expert Rev Mol Med* **18**, e7.
Tuloup-Minguez, V., Hamai, A., Greffard, A., Nicolas, V., Codogno, P. and Botti, J. (2013). Autophagy modulates cell migration and beta1 integrin membrane recycling. *Cell Cycle* **12**, 3317-3328.
Wan, J., Cheung, A. Y., Fu, W. Y., Wu, C., Zhang, M., Mobley, W. C., Cheung, Z. H. and Ip, N. Y. (2008). Endophilin B1 as a novel regulator of nerve growth factor/ TrkA trafficking and neurite outgrowth. *J Neurosci* **28**, 9002-9012.
Yang, J. S., Zhang, L., Lee, S. Y., Gad, H., Luini, A. and Hsu, V. W. (2006). Key components of the fission machinery are interchangeable. *Nat Cell Biol* **8**, 1376-1382.
Yla-Anttila, P., Vihinen, H., Jokitalo, E. and Eskelinen, E. L. (2009). 3D tomography reveals connections between the phagophore and endoplasmic reticulum. *Autophagy* **5**, 1180-1185.
Yoon, S. Y., Ha, Y. E., Choi, J. E., Ahn, J., Lee, H., Kweon, H. S., Lee, J. Y. and Kim, D. H. (2008). Coxsackievirus B4 uses autophagy for replication after calpain activation in rat primary neurons. *J Virol* **82**, 11976-11978.
Young, A. R., Chan, E. Y., Hu, X. W., Kochl, R., Crawshaw, S. G., High, S., Hailey, D. W., Lippincott-Schwartz, J. and Tooze, S. A. (2006). Starvation and ULK1-dependent cycling of mammalian Atg9 between the TGN and endosomes. *J Cell Sci* **119**, 3888-3900.
Yousefi, S., Perozzo, R., Schmid, I., Ziemiecki, A., Schaffner, T., Scapozza, L., Brunner, T. and Simon, H. U. (2006). Calpain-mediated cleavage of Atg5 switches autophagy to apoptosis. *Nat Cell Biol* **8**, 1124-1132.
Zhang, C., Li, A., Zhang, X. and Xiao, H. (2011). A novel TIP30 protein complex regulates EGF receptor signaling and endocytic degradation. *J Biol Chem* **286**, 9373-9381.

Figures

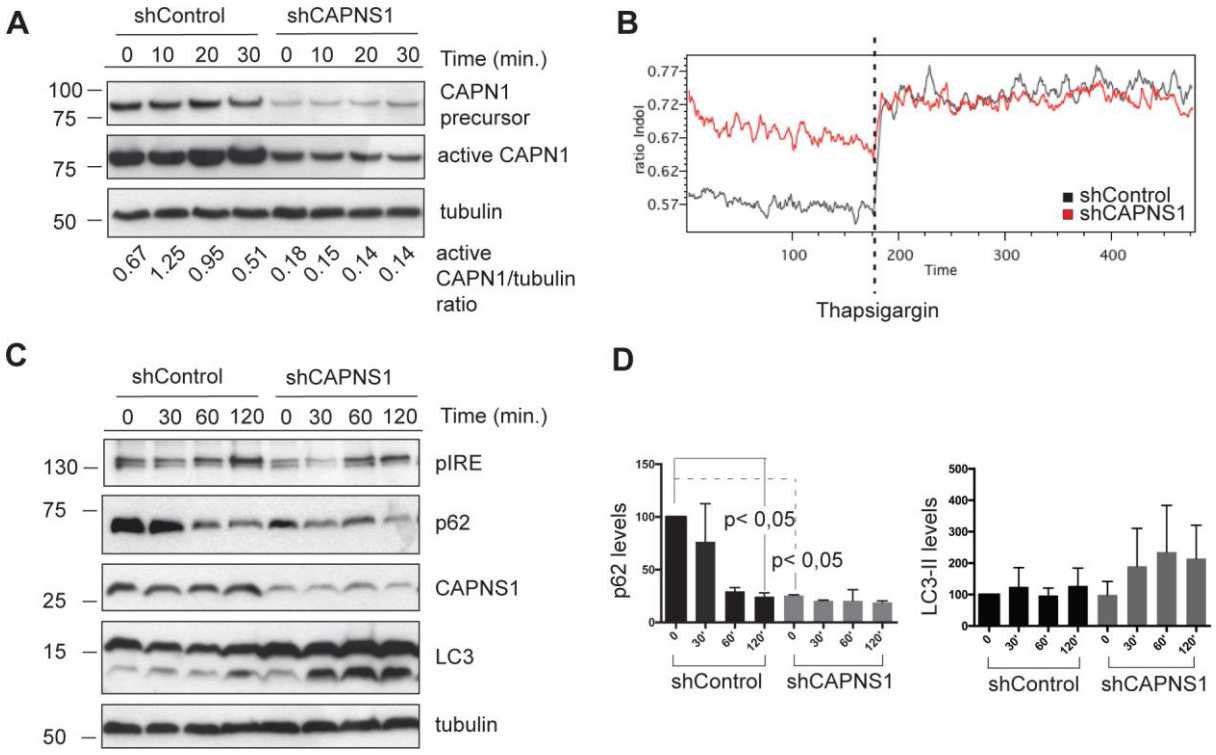

Figure 1. Thapsigargin treatment induces calpain activation and autophagy. (A) Control and shCAPNS1 cells were treated with 100 nM thapsigargin for 10, 20 and 30 minutes and the lysates subjected to Western blot analysis to quantify the precursor and the active form of CAPN1. The ratio between active CAPN1 and tubulin is reported below each lane. (B) Time course measurement of intracellular calcium concentration. The plot indicates the ratio of mean indo violet/indo blue emission values of each cell population at individual time points (minutes). The ratio corresponds to the relative calcium concentration of control and shCAPNS1 U2OS cells before and after addition of thapsigargin (100nm final). Moving average was used as smoothing method. (C) shCAPNS1 cells were treated with 100 nM thapsigargin for 30, 60 and 120 minutes and the lysates subjected to Western blot analysis to detect LC3, p62, pIRE, CAPNS1 and tubulin. (D) The graphs represent the levels of p62 and LC3 normalized to tubulin levels.

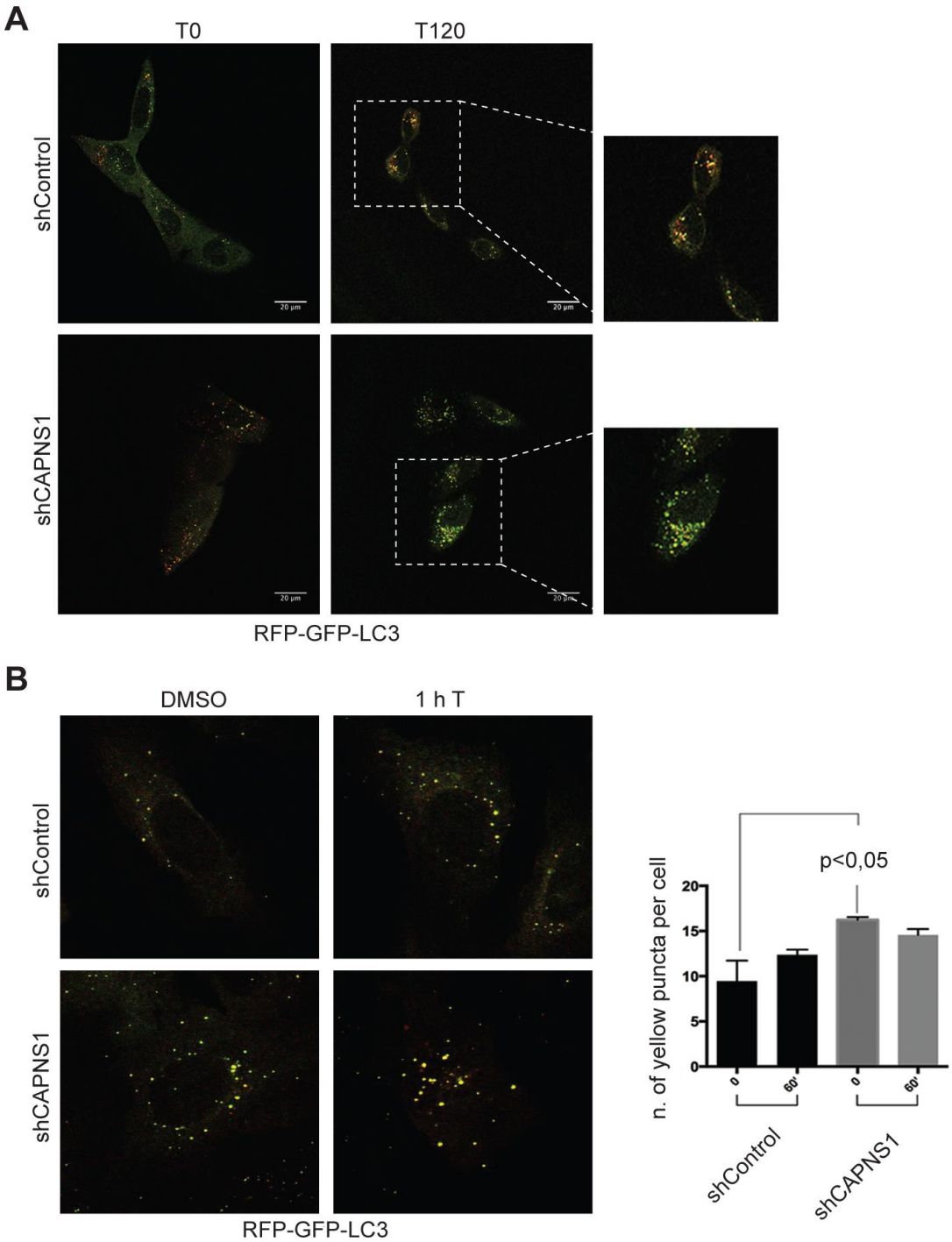

Figure 2. CAPNS1 depletion causes accumulation of LC3-II-positive structures. (A) Control and CAPNS1 depleted U2OS cells were treated with RFP-GFP-LC3 baculovirus reagent. 24 hours later, the cells were analysed under a confocal microscope over a 120 minutes time-lapse experiment. After the first 15 min., 100 nM thapsigargin was added to induce autophagy. The first (T0) and last images (T120) of the experiments are shown.

(B) Control and CAPNS1 depleted U2OS cells were treated with commercial RFP-GFP-LC3 expressing baculovirus. 24 hours later, the cells were treated with 100 nM thapsigargin or DMSO as control, for 1 hour, and then fixed and analysed. Representative confocal microscopy pictures are shown. At least 25 cells were analysed for each replica and the number of yellow dots per cell was counted. The graph reports the mean and standard deviation calculated on three independent experiments.

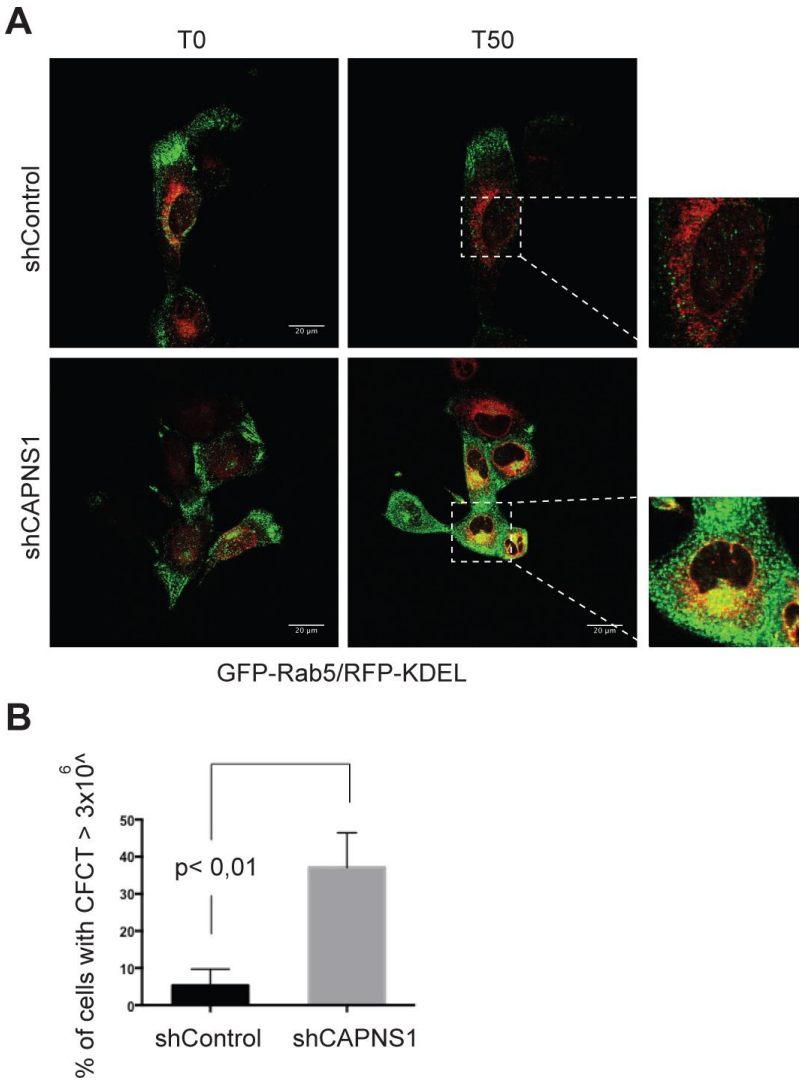

Figure 3. Early endosomes dynamics is impaired in CAPNS1 depleted cells. (A) Control and shCAPNS1 U2OS cells were grown on petri dishes, treated with commercial baculovirus reagent expressing GFP-Rab5 protein, and RFP-KDEL. 24 hours later, the cells were analysed using a confocal microscope to detect the dynamics of Rab5 positive vesicles. Images were acquired every 2 minutes over a period of 50 minutes. The first (T0) and last (T50) pictures of each time lapse experiment are shown. Scale bars correspond to 20 μM. (B) Corrected total cell fluorescence (CTCF) levels of GFP-Rab5 measured on 100 fixed control and shCAPNS1 cells. The graph indicates the percentage of cells that show a CTFC ≥ $3x10^6$; the error bars represent standard deviation of three different independent experiments; p value < 0,01.

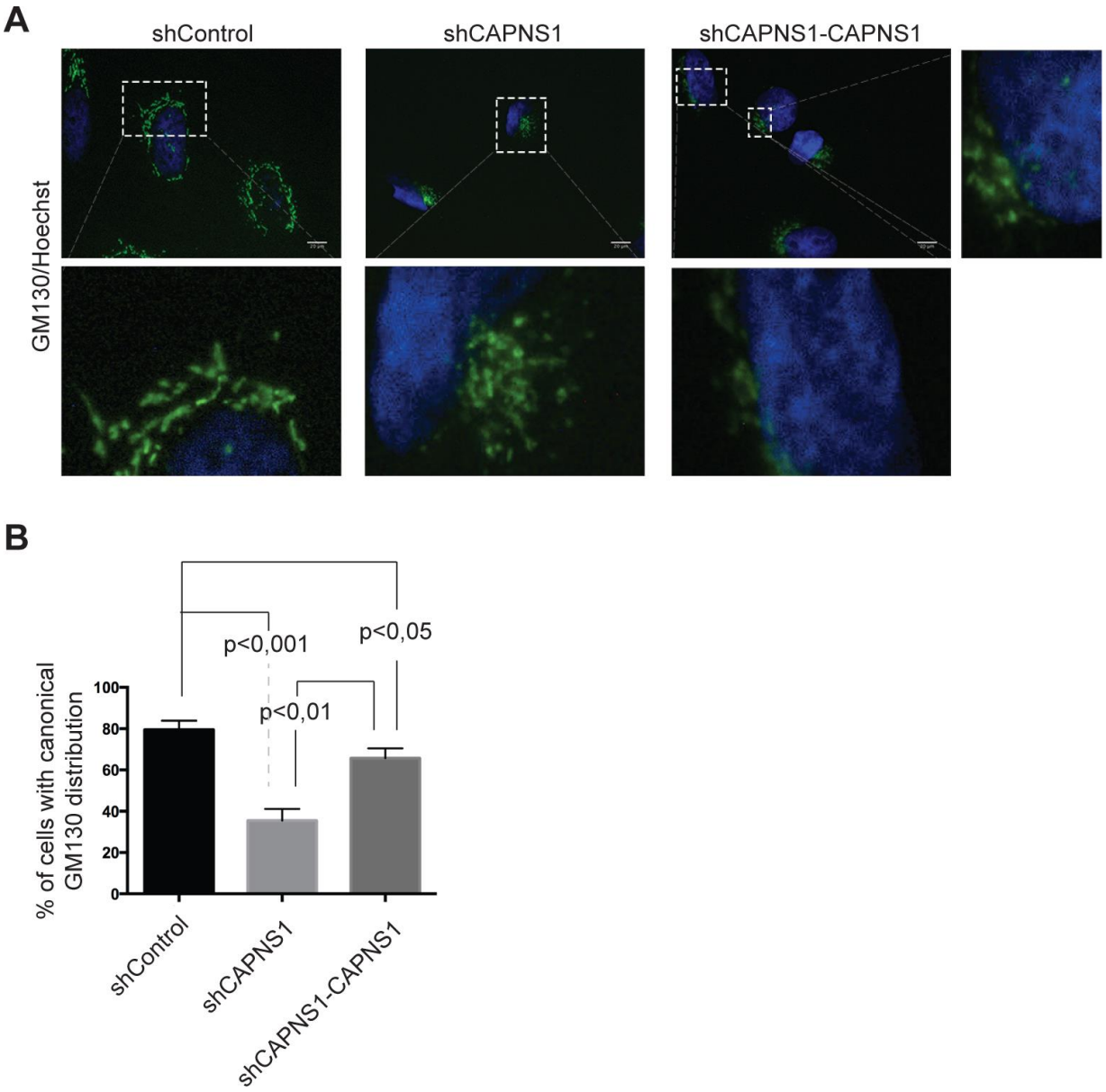

Figure 4. CAPNS1 depletion perturbs Golgi stacks distribution. (A) Control, shCAPNS1 and CAPNS1 rescued U2OS cells were fixed and stained with GM130 antibody. Hoechst die was used to decorate nuclei. A fluorescence microscope was used to acquire pictures; scale bars correspond to 20 μM. Lower and rightest panels are magnification of boxed areas. 100 cells for each sample were considered and the percentage of cells with Golgi stacks surrounding the nucleus was quantified. The graph of panel B reports the means and standard deviations of three independent experiments.

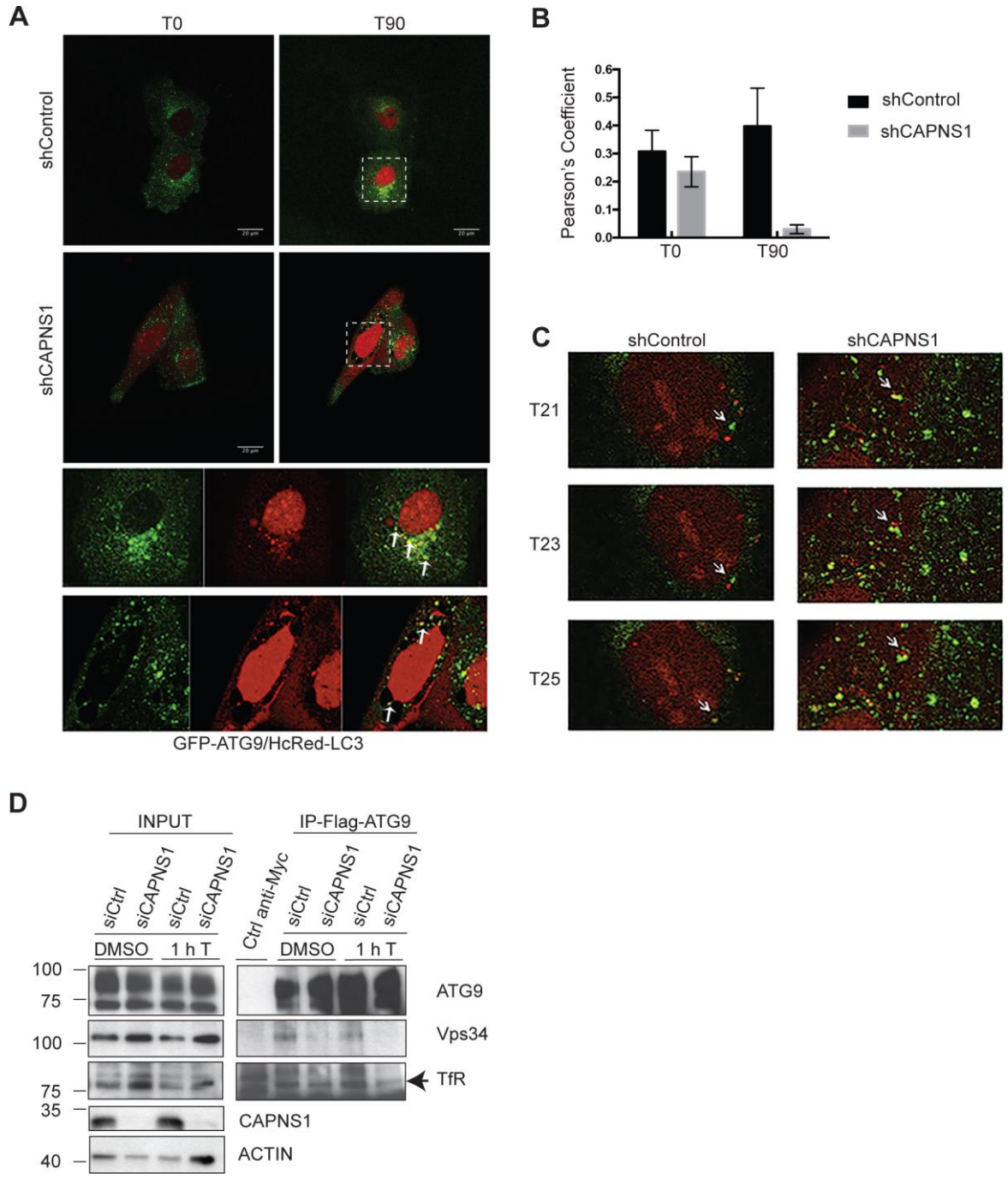

Figure 5: Atg9 dynamics is impaired in CAPNS1 depleted cells. (A) ShCAPNS1 and control cells were co-transfected with GFP-Atg9 and HcRed-LC3. 24 hours later, the cells were analysed using a confocal microscope. Images were acquired every 2 minutes over a 50 min. time interval. The first (T0) and last (T90) merged pictures of the two hours time-lapse experiments are shown. Scale bars represent 20 μM. Magnifications of boxed areas are shown in the right panels. (B) Quantification of GFP-Atg9 and HcRed-LC3 colocalization by Pearson'

coefficient determination in control and CAPNS1 depleted U2OS cells, before and after thapsigargin treatment. (C) Images sequences (T21, T23, T25) of the GFP-ATG9/HcRed-LC3 time lapse experiment made using control and CAPNS1 depleted U2OS cells. The arrow indicates one ATG9 vesicle that meets and fuses with a LC3 positive vesicle in control cells. In shCAPNS1 cells ATG9 and LC3 positive vesicles are more stationary. (D) Flag-Atg9 stably expressing U2OS cells were transfected with a CAPNS1 specific siRNA or a control siRNA. 48 hours later, the cells were treated for 1 hour with DMSO or 100 nM thapsigargin before lysis and immunoprecipitation with an anti-FLAG antibody. The immunoprecipitation products were analysed by Western blot to visualize FLAG-Atg9, endogenous TfR and Vps34.

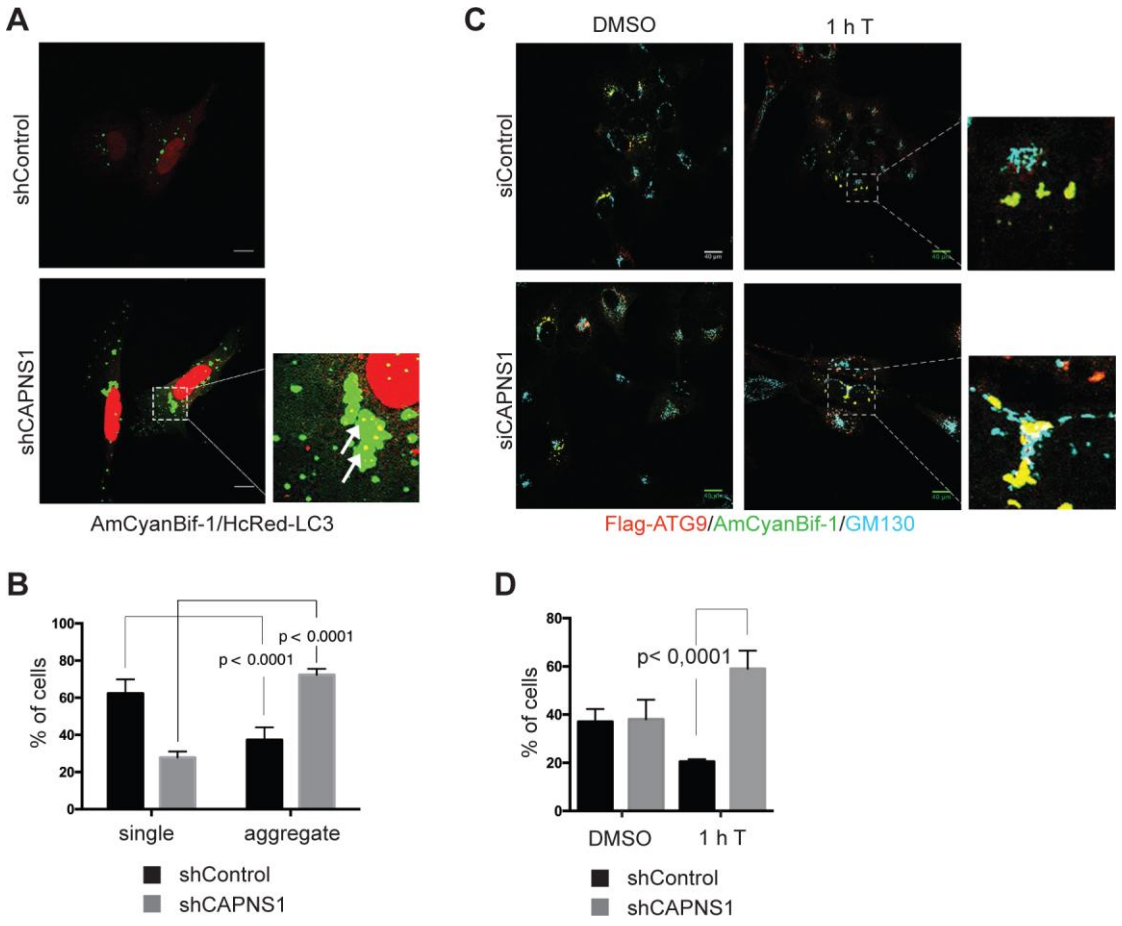

Figure 6: Atg9/Bif-1 trafficking from the Golgi is impaired in CAPNS1 depleted cells. (A) Control and shCAPNS1 U2OS cells were transiently co-transfected with AmCyan-Bif-1 and HcRed-LC3. 16 hours later, the cells were fixed and analysed by a confocal microscope. Scale bars represent 20 μM. (B) 100 cells for each sample were considered and the number of cells where Bif-1 forms aggregates or single dots was counted. The graph represents the means and standard deviations of three independent experiments. (C) U2OS cells stably expressing Flag-Atg9 were transiently silenced with control or CAPNS1 specific siRNA and then transfected with AmCyan-Bif-1. 24 h later the cells were treated for 1 h with or without 100 nM thapsigargin, and then fixed and analysed by immunofluorescence to visualize endogenous GM130, Flag-Atg9 and AmCyan-Bif1. Representative confocal merged pictures are reported in panel C; scale bars represent 20 μM. 50 cells for each sample were considered and the number of cells where Atg9/Bif-1 positive vesicles colocalizes with endogenous GM130 was counted. The graph in panel D shows the mean and standard deviation of three independent experiments.

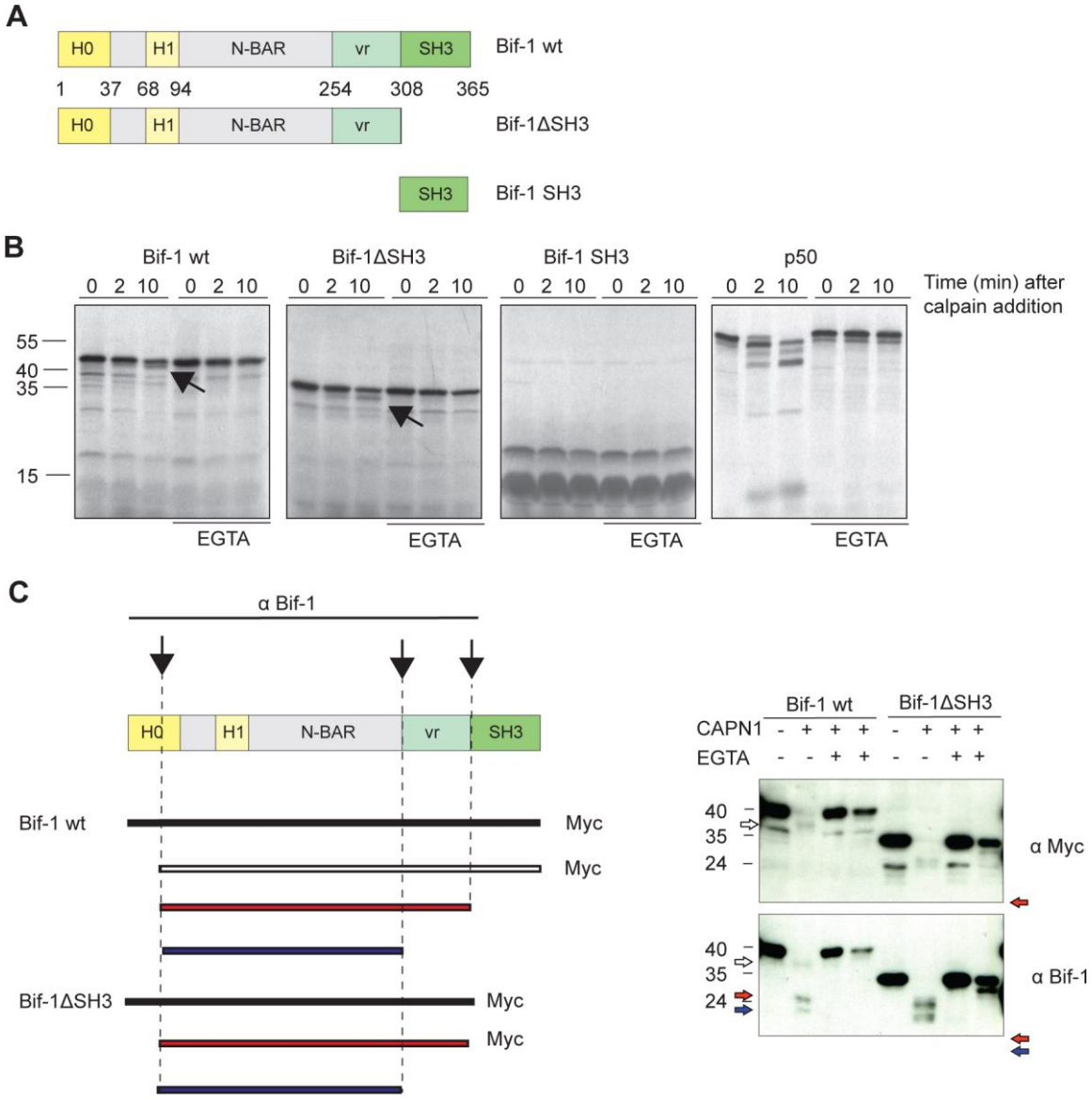

Figure 7. The N-terminal region of Bif-1 protein is cleaved by calpain. (A) Schematic representation of the structure of wild type Bif-1 and mutants. Bif-1 contains two domains involved in membrane binding: H0 and H1, a N-BAR domain and a C-terminal SH3 domain. (B) Bif-1 wt, Bif-1 ΔSH3, Bif-1 SH3 and p50 NF-κB1 were produced as ^{35}S methionine-labeled proteins by in vitro transcription and translation and incubated for the indicated time intervals with commercial micro-calpain, as previously described (Demarchi et al., 2005). The reactions were then stopped in Laemmli buffer and analyzed by SDS-PAGE and autoradiography. Parallel reactions in the presence of 10 μM EGTA were carried out to prove the calcium dependency of the reactions. Arrows indicate calpain cleavage products. (C) Schematic drawing of Bif-1 and its derivative fragments obtained after calpain cleavage and analysed by western blot anti myc

tag and anti-Bif-1 reported on the right side of the panel. The hollow arrow indicates the wt Bif-1 cleavage product retaining the SH3 domain. The solid arrows indicate lower molecular weight cleavage products lacking the C terminal SH3 domain.

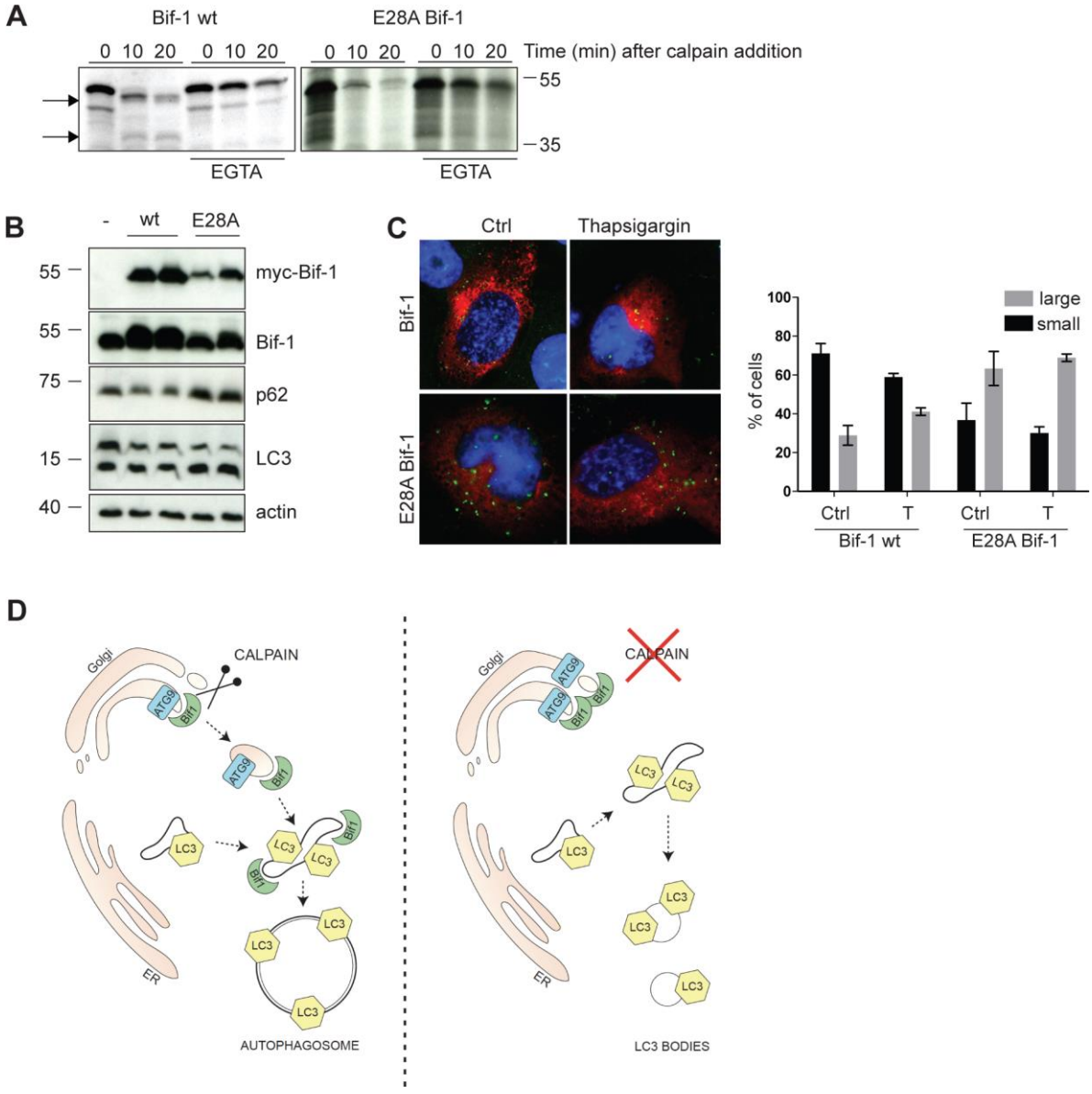

Figure 8. Aminoacid E28 on Bif-1 is important for calpain-mediated processing, and autophagic clearance of p62.

(A) Wild type Bif-1, and E28A Bif-1 were produced as ^{35}S methionine-labeled proteins by in vitro transcription and translation and incubated for the indicated time intervals with commercial micro-calpain, as previously described (Demarchi et al., 2005). The reactions were then stopped in Laemmli buffer and analysed by SDS-PAGE and autoradiography. Parallel reactions in the presence of 10 μM EGTA were carried out to prove the calcium dependency of the reactions. Arrows indicate calpain cleavage products. (B) The myc-tagged constructs: wild type Bif-1, and E28A Bif-1 were transfected into H1299 cells. 24 hours later, the cells were

treated or not with 100 nM thapsigargin for 1 hour. Afterwards, the cell lysates were prepared and analysed by western blot with the indicated antibodies. (C) The myc-tagged constructs: wild type Bif-1, and E28A Bif-1 were transfected into H1299 cells. 24 hours later, the cells were treated or not with 100 nM thapsigargin for 1 hour. Afterwards, the cells were fixed and analysed by immunofluorescence using anti-myc and anti-LC3 antibodies. Anti-myc is stained in red, endogenous LC3 is stained in green. Scale bars correspond to 20 μM. The graphs show the percentage of cells with small/large LC3 dots. The error bars represent standard deviation of three different independent experiments. At least 25 cells were analysed for each replica

(D) Working model: Calpain processes Bif-1, and allows delivery of Atg9-Bif-1 vesicles to the nascent autophagosome. In the absence of calpain, LC3 positive bodies accumulate in the cells.

SUPPLEMENTARY FIGURES

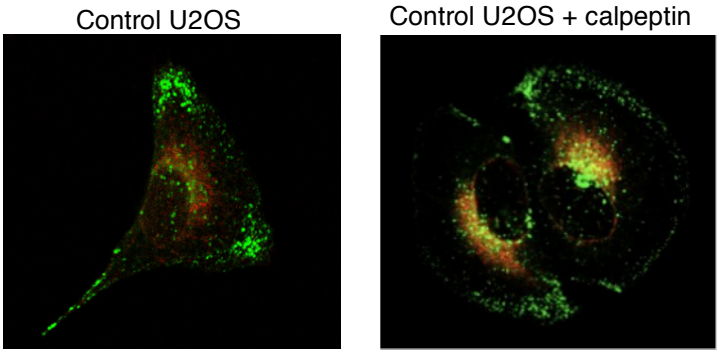

Fig. S1: Early endosomes dynamics is perturbed upon calpain inhibition. Control U2OS cells were incubated with commercial GFP-Rab5 and RFP-KDEL-calreticulin expressing reagents. 12 h after treatment, the cells were left untreated or treated for 2 h with 0,5 mM Calpeptin, a calpain inhibitory peptide. Samples were then fixed and analyzed under a confocal microscope. Representative fields are shown.

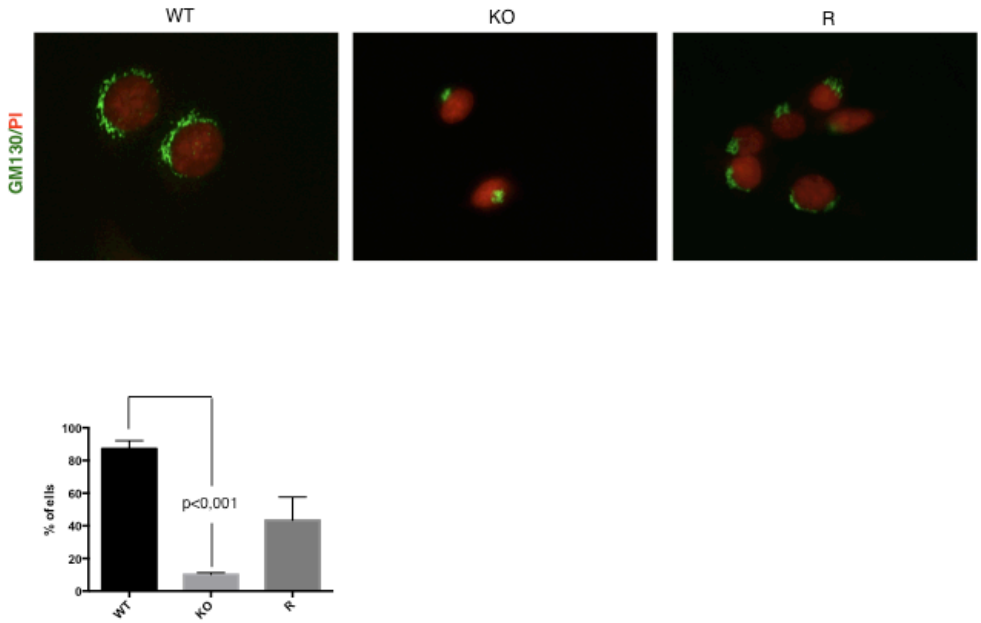

Fig. S2 Calpain activity is coupled to Golgi redistribution

S2A. Wild type (WT), CAPNS1 knock out (KO) and rescued (R) MEFs were fixed and stained with GM130 antibody. Propidium iodide was used to decorate nuclei.100 cells for each sample were considered and the percentage of cells with canonical distribution of the Golgi apparatus was counted and is reported in the graph. In CAPNS1 ko MEFs, GM130 appears concentrated on one site.

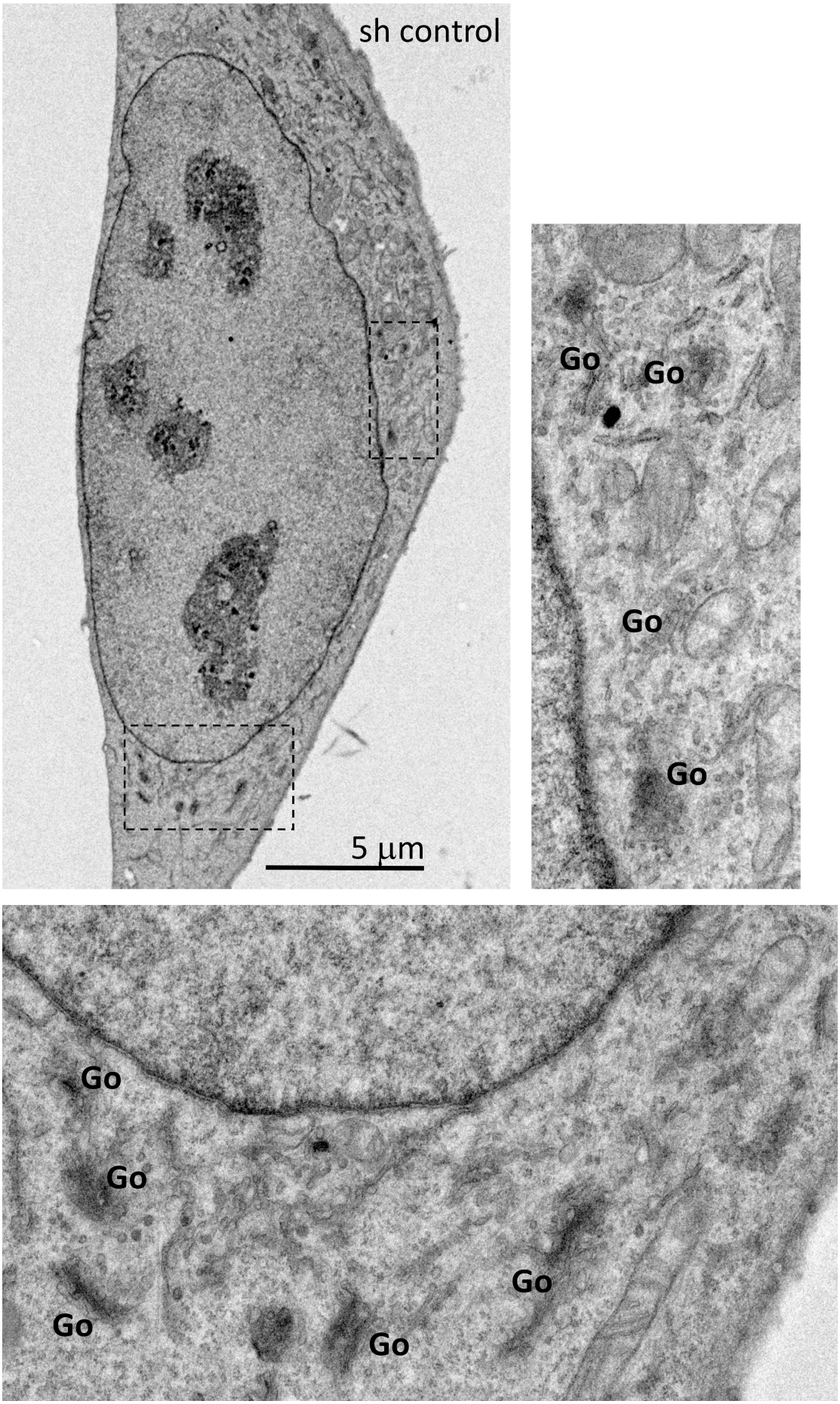

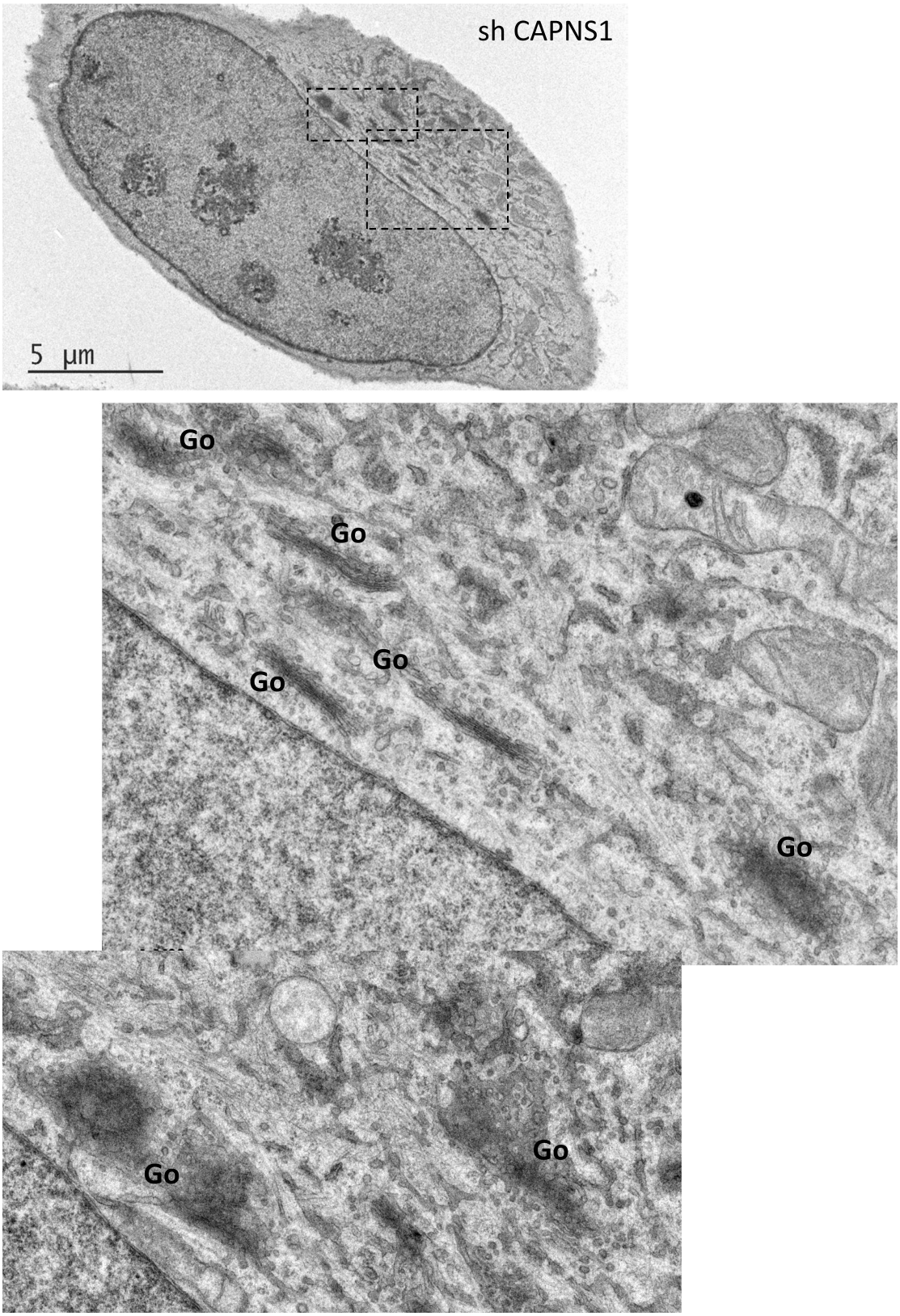

Figure S2 B: Representative electron microscopy micrographs of control (sh control) and CAPNS1 depleted (sh CAPNS1). Boxed areas are shown at higher magnification. In control cells Golgi distributes all around the nucleus; while in CAPNS1 depleted cells, it is mainly found at one side of the nucleus. Golgi stacks are labeled: Go.

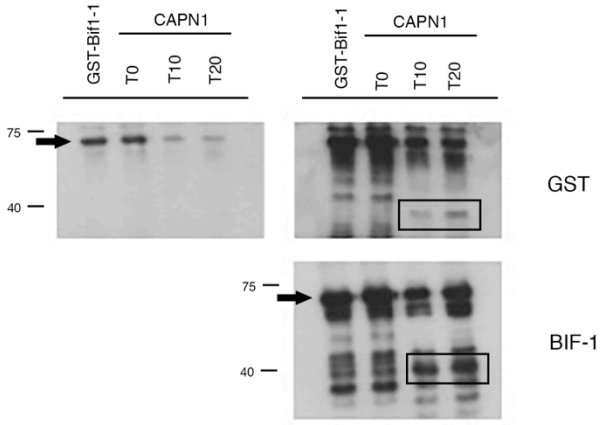

Fig. S3: Bif-1 protein is cleaved by calpain. In vitro cleavage of GST-Bif-1**.** Briefly, GST-Bif-1, expressed and purified from E. coli, was incubated for the indicated time: 0, 10 or 20 minutes, with commercial CAPN1. The cleavage products were analysed by Western blot analysis with anti-Bif-1 and anti-GST antibodies. The GST antibody recognizes a cleavage product at an apparent molecular weight of about 30 kD, roughly few kilodaltons heavier than GST alone. The anti-Bif-1 antibody, on the other hand, detects another band of molecular weight compatible with Bif-1 lacking the N-terminal end. Arrows indicate Full length GST-Bif-1; rectangular shapes surround the cleavage products.

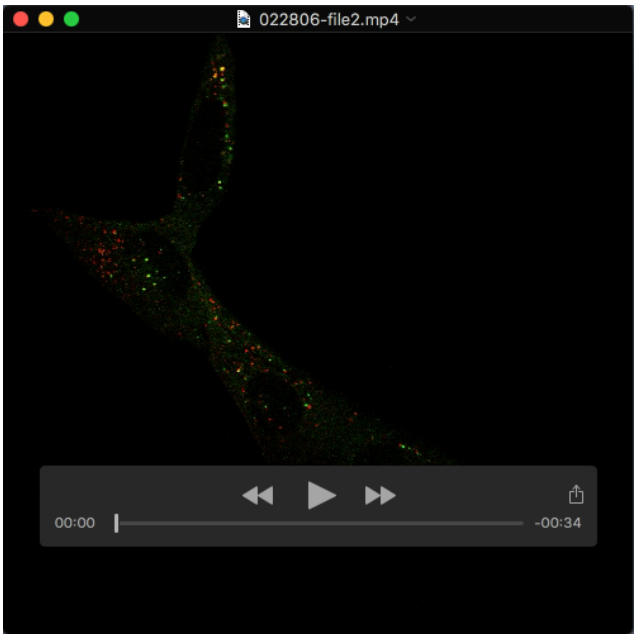

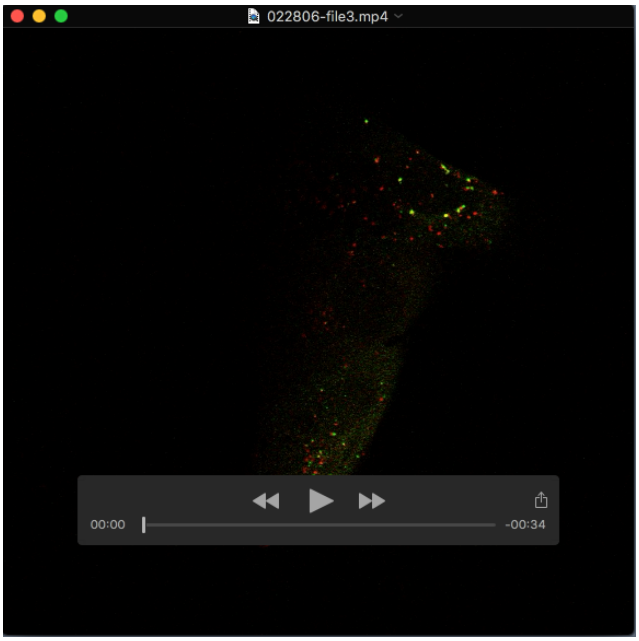

Movies 1,2. CAPNS1 depletion is coupled to an accumulation of LC3-II-positive structures. Control (Movie 1) and shCAPNS1 U2OS cells (Movie 2) were incubated with commercial baculoviruses expressing RFP-GFP-LC3. 24 hours later, a 2 hours time-lapse experiment was performed using a confocal microscope. After the first 15 minutes of images acquisition, 100 nM thapsigargin was added to the cells. Images were acquired every two minutes.

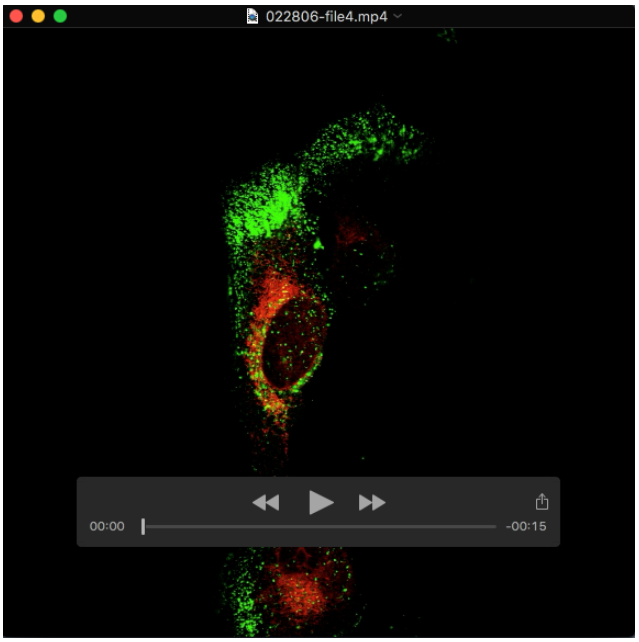

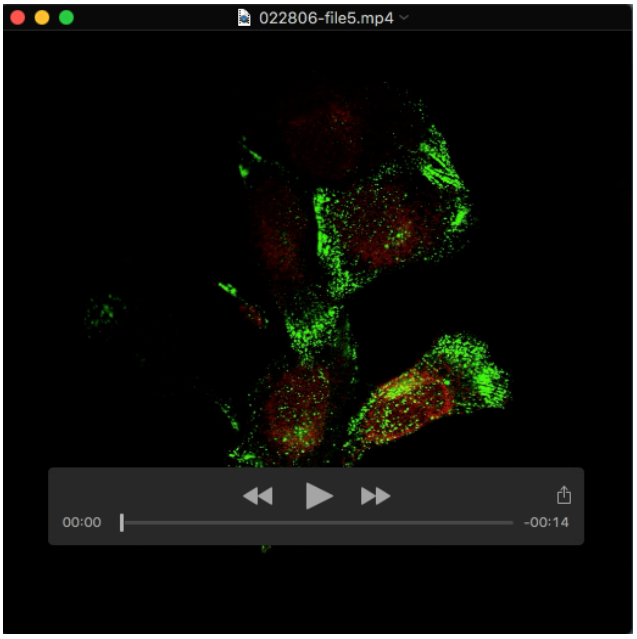

Movie 3,4. Early endosomes dynamics is perturbed in CAPNS1 depleted cells. Control (Movie 3) and shCAPNS1 U2OS cells (Movie 4) were incubated with commercial baculoviruses expressing GFP-Rab5 and KDEL-RFP. 24 hours later, a 50 minituse time-lapse experiment was performed using a confocal microscope. After the first 15 minutes of images acquisition, 100 nM thapsigargin was added to the cells. Images were acquired every two minutes.

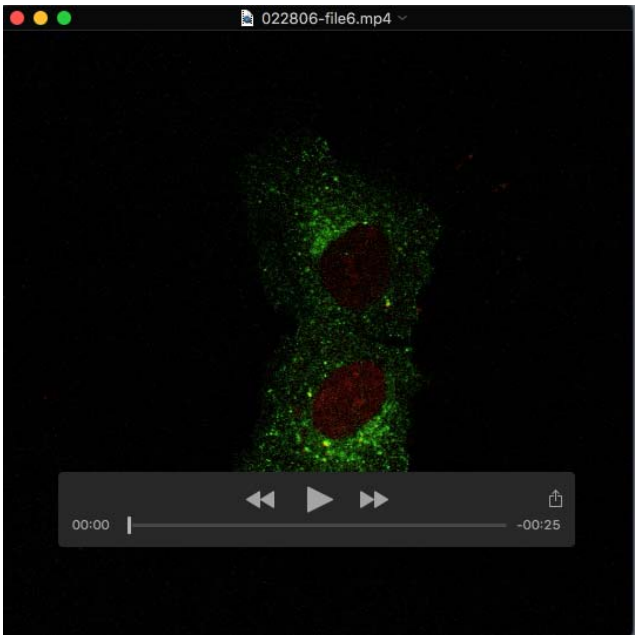

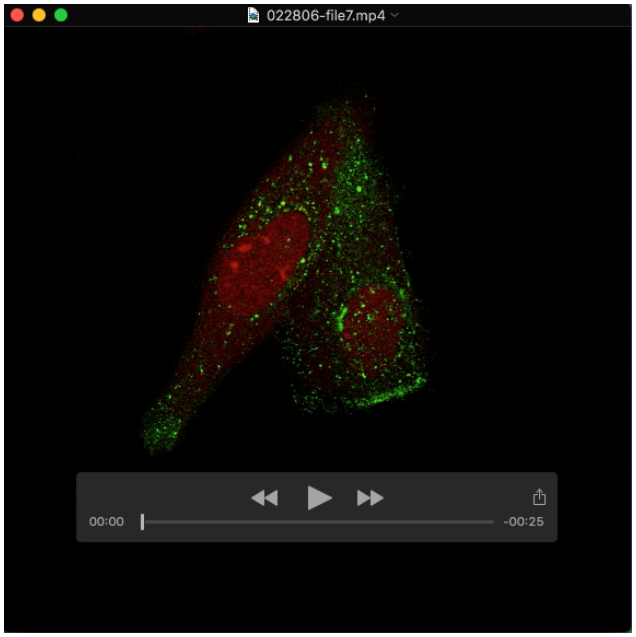

Movie 5,6. CAPNS1 depletion is coupled to impairment of Atg9 traffic. Control (Movie 5) and shCAPNS1 U2OS cells (Movie 6) were transfected with HcRed-LC3 and GFP-Atg9. 24 hours later, a 90 minutes time-lapse experiment was performed using a confocal microscope. After the first 15 minutes of images acquisition, 100 nM thapsigargin was added to the cells. Images were acquired every two minutes.